Composite Structures 382 (2026) 120089

Contents lists available at ScienceDirect

Composite Structures

journal homepage: www.elsevier.com/locate/compstruct

Limits of analytical models of sandwich structures for optimization

Vladimír Hostinský [a,*], Jurij Sodja [b], Ivo Jebáček [a], Jan Navrátil [a]

[a] Institute of Aerospace Engineering, Brno University of Technology, Technická 2896/2, Brno, 616 69, Czechia
[b] Aerospace Structures and Materials, Technical University Delft, Kluyverweg 1, Delft, 2629 HS, Netherlands

ARTICLE INFO

Dataset link: DOI: 10.5281/zenodo.14229746, DOI:10.5281/zenodo.18377054

Keywords:
Metamaterials
Honeycombs
Aeroelastic tailoring
Sandwich panel
Optimization

ABSTRACT

Current advances in the structural optimization of aircraft structures have led to the introduction of sandwich panels into the optimization process. This study attempts to extend the possibilities of sandwich optimization by proposing an analytical model which predicts the homogenized properties of a sandwich panel with a honeycomb core and CFRP skins. The model is based on a combination of Classical laminate theory and a 1-D beam model of the honeycomb core. The finite-element equivalent of tensile and shear tests is used to validate the proposed model on a broad range of core geometries with different combinations of core thickness, wall angle, cell elongation, and cell wall thickness. The results of 425 different geometries showed the overall precision of the proposed model, highlighted effects in the behavior of the core that drive the sandwich properties further from the predicted values, and suggested which parts of the model are suitable for optimization and where are their limits of applicability.

1. Introduction

Increasingly progressive approaches to aircraft conceptual design are emerging across academia and industry [1–3]. Created as a direct outcome of the current effort for more economical and environmentally conscious aviation [4], they often feature aerodynamically efficient, highly flexible, slender wings, which are pushing structural design possibilities to their limits [5–7]. Together with a constant drive towards weight minimization, omnipresent in the aerospace industry, these new trends create a need to fully exploit the potential of any material used in the wing structure. This can be achieved not only through an optimal shaping of the structural components of the wing, but also through precise optimization of the properties of the material itself. The latter approach, traditionally associated with a design of fiber-composite structures [8], has already become an integral part of the aerospace design process in the form of *aeroelastic tailoring*.

As in any other optimization process, the results of aeroelastic tailoring are shaped by the optimization objective and the constraints included in the optimization. Consequently, the choice of a suitable set of constraints marks a difference between a realistically optimized design and an overly optimistic one. Recent studies including the works of Brooks et al. [9], Wang et al. [10] and Sodja et al. [11] identify buckling as one of the main constraints driving the results of aeroelastic tailoring. The tendency of panels to buckle is mainly influenced by their flexural stiffness, which in turn increases with the cube of the thickness of the optimized laminate [12].

Use of a sandwich consisting of a low-density core and stiff faces instead of the monolithic laminate proves to be one of the most beneficial ways to increase the flexural stiffness of the structure while avoiding the weight penalty associated with an increase in the number of layers in the laminate [13]. Previous research introducing sandwich optimization into the context of aeroelastic design is limited to the use of a core with fixed properties [14], a core with variable thickness [15,16], and a core made of functionally graded foam [17]. Apart from the later, neither of these approaches explores the possibilities that could be achieved with more complex core materials and core structural optimization.

In light of recent developments in additive manufacturing and computer-driven manufacturing in general, leaving the core of the structure unoptimized presents a missed opportunity. With additive manufacturing in mind, the mechanical properties of some artificially designed cellular materials can be optimized by modifying the geometry of their material cells. Generally referred to as mechanical metamaterials [18–20], they already proved the benefits of their use [21].

The approach used in the design of metamaterials can be applied to the design of a honeycomb structure, one of the traditionally used sandwich core materials. A change in any of the geometrical parameters defining the honeycomb structure leads to a significant difference in the overall mechanical properties of the sandwich core [22], creating a sandwich more suitable for its intended use [23]. Core optimization on the material level combined with simultaneous optimization of

* Corresponding author.
E-mail address: Vladimir.Hostinsky@vutbr.cz (V. Hostinský).

https://doi.org/10.1016/j.compstruct.2026.120089
Received 29 September 2025; Received in revised form 24 December 2025; Accepted 20 January 2026
Available online 21 January 2026

fiber layout of sandwich faces could not only increase the flexural stiffness while ensuring minimal weight penalty, but also serve to minimize the effects of sandwich-specific failure modes, such as wrinkling, intercellular buckling, or core crushing.

The analytical nature of currently available models of homogenized mechanical properties of honeycomb core [24–26] could allow convenient integration with lamination-parameters based description of hybrid panels as proposed by Silva et al. [27]. A fixed number of design variables used within this combination of models allows its use with a gradient-based optimizer, which is frequently used in the preliminary design optimization of aerospace structures [28,29].

Two major problems arise from the implementation of the analytical models of honeycomb core into the homogenized representation of the sandwich panel. Firstly, the precision of the models was usually verified only on a limited number of honeycomb geometries, which do not necessarily represent the broad design space available to the honeycomb structure. Secondly, all the models are based on a variation of the 1D beam theory, which inevitably neglects three-dimensional deformations arising from a significant imparity between the stiffness of the core and that of the skins.

The significance of these effects (and thus also the precision of predicted sandwich properties) varies throughout the design space of the honeycomb core, and consequent limits of validity of the mentioned models were never properly identified. This study presents a novel modeling approach based on a combination of existing analytical models. Novelty of this model combination and the proposed future use within structural optimization process creates the necessity to find its limits of applicability. Authors do so by comparing the resulting homogenized mechanical properties obtained by the analytical approach with results obtained by the numerical approach in the form of finite element analysis (FEA) conducted on a large number of different core geometries logically distributed across a selected design space.

2. Methods

The proposed approach of obtaining homogenized properties of a sandwich panel can be divided into two submodels, one describing the behavior of the skins and the other representing the core. In accordance with the Classical Laminate Theory (CLT), both submodels use A, B, and D stiffness matrices to represent the resulting stiffness of the corresponding component. To obtain a single set of stiffness matrices of the entire sandwich panel, the component matrices are transposed using offsets integrated into CLT as described later.

2.1. Skin submodel

To maintain a fixed number of design variables and allow the use of a gradient-based optimizer, the skin submodel uses lamination parameters. This approach, already in frequent use in aeroelastic tailoring [11,28,30], was first proposed by Tsai and Hahn [31] in 1968. It uses 12 lamination parameters, 5 material invariants, and a skin thickness to fully describe any laminate layout. The lamination parameters can be divided into three types corresponding to the in-plane, out-of-plane, and coupled stiffness of the laminate. To allow their calculation for a sandwich skin consisting of N laminate plies of a constant thickness, the original definition of lamination parameters can be rewritten to the following equations presented by Macquart et al. [30]:

$$V_1^A, V_2^A, V_3^A, V_4^A = \frac{1}{N}\sum_{n=1}^{N} cos2\theta_i, sin2\theta_i, cos4\theta_i, sin4\theta_i \quad (1)$$

$$V_1^B, V_2^B, V_3^B, V_4^B = \frac{2}{N^2}\sum_{i=1}^{N} (Z_i^2 - Z_{i-1}^2)(\cos 2\theta_i, \sin 2\theta_i, \cos 4\theta_i, \sin 4\theta_i) \quad (2)$$

$$V_1^D, V_2^D, V_3^D, V_4^D = \frac{4}{N^2}\sum_{i=1}^{N} (Z_i^3 - Z_{i-1}^3)(\cos 2\theta_i, \sin 2\theta_i, \cos 4\theta_i, \sin 4\theta_i) \quad (3)$$

where $Z_i = -N/2 + i$ and θ_i is the fiber angle of the ply i.

Required stiffness matrices of the skins are obtained from the lamination parameters using the approach proposed by Tsai and Pagano in [31].

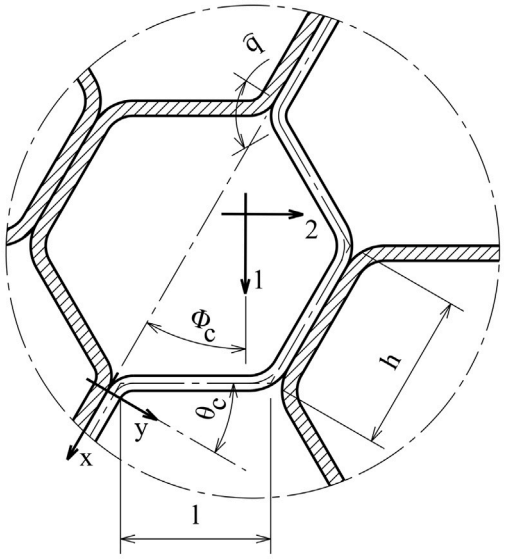

Fig. 1. Honeycomb core geometry.

2.2. Parametrized model of the core

The honeycomb core geometry can be fully described by a set of seven parameters listed in Table 1 and for clarity also shown in Fig. 1.

When combined with the properties of the bulk material of the core, these parameters can be used to predict the homogenized mechanical properties of the core. The two most widely used models that allow this prediction were created by Masters & Evans [25] and Gibson et al. [22], the latter of which was further refined by Malek & Gibson [24].

Comparison of the two models against a series of FE models of honeycomb cores with different $t/l, h/l$ and θ showed, that although the more complex Master's model considers additional modes of deformation of the honeycomb structure, the resulting Young's moduli E_{11} delivered by Gibson's model were more accurate. In light of these results, which are partially presented in Fig. 2, the study proceeded using Gibson's model only.

Malek & Gibson's model is based on a solution of one-dimensional beam theory and offers a set of equations [24] to estimate the homogenized properties of the core, consisting of the two in-plane moduli E_X and E_Y, in-plane shear modulus G_{XY} and Poisson's ratio ν_{XY} which correspond with the coordinate system of the core (x, y in Fig. 1). To keep the denotations consistent throughout the study, the equations can be rewritten into the following form:

$$E_X = E_s\left(\frac{t}{l_b}\right)^3 \frac{h/l + sin\theta_C}{cos^3\theta_C} \cdots \left(\frac{1}{1 + \left(2.4 + 1.5\nu_s + tan^2\theta_C + \frac{(h_b/l_b)}{cos^2\theta_C}\right)(t/l_b)^2}\right) \quad (4)$$

$$E_Y = E_s(t/l_b)^3 \frac{cos\theta_C}{(h/l + sin\theta_C)sin^2\theta_C}\left(\frac{1}{1 + (2.4 + 1.5\nu_s + cot^2\theta_C)(t/l_b)}\right) \quad (5)$$

$$\nu_{XY} = \frac{sin\theta_C(h/l + sin\theta_C)}{cos^2\theta_C}\left(\frac{1 + (1.4 + 1.5\nu_s)(t/l_b)^2}{1 + (2.4 + 1.5\nu_s + tan^2\theta_C + \frac{2(h_b/l_b)}{cos^2\theta_C})(t/l_b)^2}\right) \quad (6)$$

$$G_{YX} = E_s\left(\frac{t}{l_b}\right)^3 \frac{h/l + sin\theta_C}{(h_b/l_b)^2 cos\theta_C}\left(\frac{1}{C}\right) \quad (7)$$

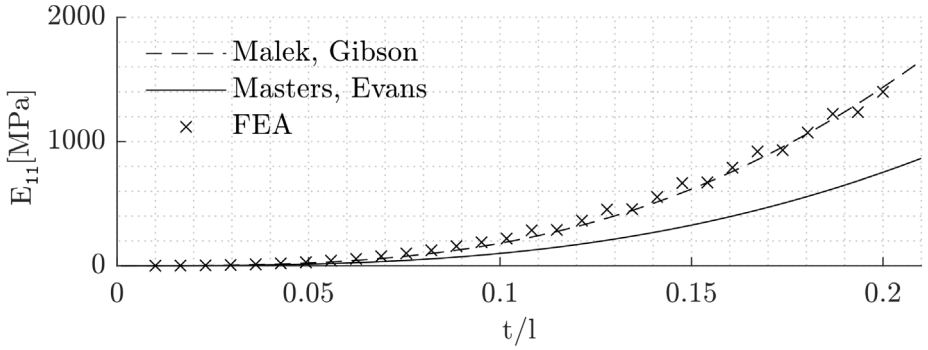

Fig. 2. Comparison of E_{11} obtained using the two analytical models and FE models for honeycomb cores with different t/l.

Table 1
Geometric parameters describing the honeycomb core.

Double wall length	h	[mm]
Inclined wall length	l	[mm]
Wall thickness	t	[mm]
Core thickness	b	[mm]
Cell angle	θ_C	[°]
Core orientation within a sandwich	Φ_C	[mm]
Corner bend length	q	[mm]

where:

$$l_b = l - t \cdot tan\left(\frac{\pi}{4} - \frac{\theta_C}{2}\right) \tag{8}$$

$$h_b = h - t \cdot tan\left(\frac{\pi}{4} - \frac{\theta_C}{2}\right) \tag{9}$$

$$C = 1 + 2(h_b/l_b) + (t/l_b)^2\left(\frac{2.4 + 1.5\nu_s}{h_b/l_b}(2 + (h/l) + sin\theta_C)\right) \ldots + \frac{h/l + sin\theta_C}{(h_b/l_b)^2}((h/l + sin\theta_C)tan^2\theta_C + sin\theta_C) \tag{10}$$

To obtain homogenized stiffness matrices of the core $\mathbf{A_C}$, $\mathbf{B_C}$ and $\mathbf{D_C}$ corresponding to the main material coordinate system (1, 2 in Fig. 1), the core is treated as a single ply laminate with a ply angle ϕ_c, for which homogenized stiffness matrices of the core are calculated by following the process described in detail by Barbero in [32].

Reduced stiffness matrix of the ply $\mathbf{Q}$ is calculated using the homogenized properties from Eqs. (4)–(7) and then transformed into the X, Y coordinate system using the transformation matrix $\mathbf{T}$ with the ply angle ϕ_c. Considering the lamina representing the sandwich core has a single ply, and the stiffness properties are calculated with respect to its middle plane, the transformed stiffness matrix $\overline{\mathbf{Q}}$ of the ply can be turned into a full set of homogenized stiffness matrices of the core using the following equations:

$$\mathbf{A_C} = \overline{\mathbf{Q}} \cdot b \tag{11}$$

$$\mathbf{B_C} = 0 \tag{12}$$

$$\mathbf{D_C} = \overline{\mathbf{Q}} \cdot \frac{b^3}{12} \tag{13}$$

where b denotes the core thickness.

2.3. Sandwich representation

The stiffness matrices of the sandwich core and skins are calculated with respect to the central plane of the given sandwich component. Silva and Meddaikar [27] present an approach to create a single set of stiffness matrices representing the homogenized properties of the sandwich panel. The matrices $\mathbf{B}$ and $\mathbf{D}$ of each sandwich component are offset by the distance between the sandwich central plane and the relative position of the central plane of the component. Coupling matrices $\mathbf{B}_U$ and $\mathbf{B}_L$ correspond to the upper and the lower skin respectively. To obtain $\mathbf{A}$, $\mathbf{B}$, and $\mathbf{D}$ matrices of a sandwich with a single core material and two skins of equal thickness, the original equations proposed by Silva and Meddaikar can be rewritten in the following way:

$$\mathbf{A} = \mathbf{A}_C + \mathbf{A}_U + \mathbf{A}_L \tag{14}$$

$$\mathbf{B} = \mathbf{B}_U - \frac{h_O}{2}\mathbf{A}_U + \mathbf{B}_L + \frac{h_O}{2}\mathbf{A}_L \tag{15}$$

$$\mathbf{D} = \mathbf{D}_C + \mathbf{D}_U + \mathbf{D}_L + h_O\left(\mathbf{B}_L - \mathbf{B}_U\right) + \frac{h_O^2}{4}\mathbf{A} \tag{16}$$

where h_0 is the offset thickness, which can be calculated as follows:

$$h_0 = \frac{T}{2} + \frac{b}{2} \tag{17}$$

where T is the skin thickness.

2.4. FE validation

Experimental approach [22,25] and FE analysis of a simplified representative volume element (RVE) subjected to symmetry constraints [24,26] are the most common ways to validate the analytical model of a lattice structure. The scope of the experimental approach is inevitably limited by the number of available samples, while the RVE approach often leads to simplifications similar to the ones used in the evaluated analytical model. To avoid these limitations, this study uses high resolution FE shell model of the tested sandwich panels to create a virtual equivalent of tensile and shear tests, which allows evaluation across a broad range of parameters governing the properties of such sandwich panels while capturing phenomena that are neglected in the analytical model such as thickness effect [33], axial elongation of a cell wall or the corner deformation effects [25].

Three separate FE meshes subjected to different loading conditions, shown in Fig. 3, are created for each of the tested sample panels. The two tensile setups, denoted as (a) and (b), are used to determine two Young's moduli of the panel. The third setup, denoted (c), allows shear testing to determine the homogenized shear modulus. During the analysis, the FE model of the tested sandwich panel is fixed by a zero displacement condition on one edge while being subjected to predefined displacements δ on the opposing edge. The homogenized moduli are estimated from the reaction force denoted F, which acts on the constrained edge of the sample in a reaction to the predefined displacement.

Poisson's ratios ν_{12} and ν_{21} are calculated using transverse deformation estimated during the tensile testing as an average of deformations measured at three predefined cross-sections marked I.-III. in Fig. 3.

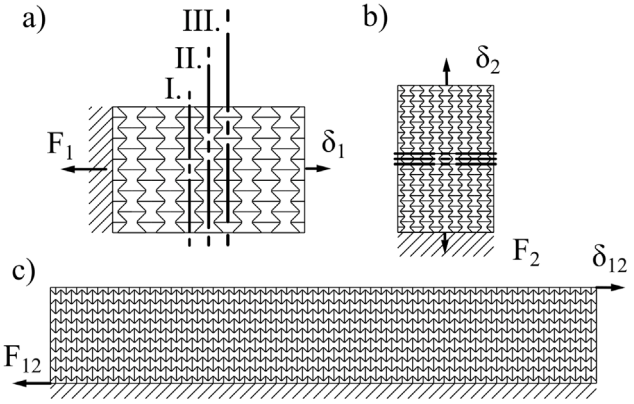

Fig. 3. Used analysis setups.

Table 2
Validation sampling overview.

Variable		Min.	Max.	Samples
Height over length of a cell	h/l	0.5	3	3
Wall thickness over length of a cell	t/l	0.05	0.3	6
Core thickness	b	2 mm	30 mm	5
Cell wall angle	θ_c	−60°	+60°	6

Table 3
Fixed parameters of core (left) and skin (right). Index S marks properties of a bulk material of the core.

l	10 mm	Upper skin layout	Single ply [0°]
ϕ_c	0°	Lower skin layout	Single ply [0°]
q	$0.3 * l$	T	0.1 mm
E_S	70 GPa	E_{11SK}	125 930 MPa
G_S	26 GPa	E_{22SK}	7720 MPa
ν_{12S}	0.33	G_{12SK}	3610 MPa
		ν_{12SK}	0.336

2.4.1. Sample selection

To reduce the number of analyzed cases to a manageable value, the number of design parameters of the honeycomb core was reduced to the four listed in Table 2 — a simplification based on the results of Gibson and Ashby [34], who demonstrated that the scale of the core cells has relatively little influence on the resulting homogenized properties of the core, as opposed to the highly influential change in relative density of the core and the cell shape. This allows fixing the inclined wall length l to a constant value and changing the double wall length h and wall thickness t into relative values by dividing them by l.

Final selection of sample panel geometries was based on the design of experiment approach [35] with number of samples evenly distributed between the limits presented in Table 2. After applying a geometrical limit that excludes the geometrically impossible combinations of parameters (expressed in Eq. (18)), the resulting number of sample panels was reduced to a total of 425.

$$\frac{h}{l} > \frac{t}{l} - 2sin(\theta_c) \tag{18}$$

Aluminium core and CFRP skins are used throughout the study to bring the evaluated design space close to that used in practical applications. Geometrical parameters and material properties of the skins and core, which remained constant during the analysis, are listed in Table 3.

2.4.2. Sample sizes

The sample size for tensile testing of honeycomb cores (and lattice structures in general) is most commonly defined by the number of cells along the two edges of the sample. Considering the range of core parameters tested in this study, fixing the number of cells to a constant value would lead to a significant variation in the aspect ratios of different samples, which, as the results of the two sensitivity analyses presented in Fig. 4 show, has more significant effect on the analysis results than the number of cells. To balance the precision and the necessary computational effort, the minimum sample size is limited to 5×5 cells, and the aspect ratio is restricted to a value between 1.5 and 1.6, with the longer edge parallel to the loading direction. The range of values is given to avoid samples without a whole number of cells.

The effect of sample aspect ratio is even more significant on the results of shear analysis as shown in Fig. 5. Considering the significant increase in necessary computational time associated with the further increase in the aspect ratio of the sample, the minimum possible ratio of the sample is set to 5.

2.4.3. FE model

Three separate FE models shown in Fig. 3 are created for each sample geometry using a dedicated MATLAB program written by the authors [36]. Each of the created models is passed to the MSC Nastran to perform the analysis, and the results of the analysis are returned to the MATLAB environment to be evaluated.

The mesh representing the core of the sandwich consists of rectangular shell elements with a prescribed maximum size defined by a ratio between the element size and the length of a bend in the cell corner q (shown in Fig. 1) to ensure the geometry of the bend is resolved with sufficient accuracy. A mesh convergence study conducted on a mesh of a core without skins with cell wall angle $\theta_c = 30°$ proved that the ratio of 0.33 would be sufficient. To account for differences in core geometries, a more conservative ratio of 0.25 was used throughout the study, dividing the selected bend length into 4 elements. The use of 3D elements to model the core was considered and tested, but the necessity to use multiple elements across the cell wall thickness inevitably leads to a large increase in the total number of elements in the model, rendering the necessary computational effort impractically high.

Skin mesh is created by a Delaunay triangulation-based algorithm developed by Persson and Strang [37]. To ensure that the adjacent elements of the core and skin meshes are connected, the nodes on the edge of the core mesh are used as fixed seed points while creating the skin mesh. An example of such a mesh in Fig. 6 shows the use of a gradient change of mesh density, which helps to reduce the necessary computational effort by reducing the mesh density further from the core walls.

A ratio between two times the radius of the largest inscribed circle and the smallest circumscribed circle of each element is evaluated after each attempt to create the skin mesh to ensure sufficient quality of the triangular mesh [38]. A minimum ratio of 0.5 proved to be sufficient to perform the described FE analysis.

To fix one edge of the sample as shown in Fig. 3, nodes on the edge of the mesh are fixed by a zero displacement condition distributed by a multi-point constraint (MPC), while the ones on the opposing side are subjected to a forced displacement of $\delta = 10\nu\epsilon$ in the prescribed loading direction with the same method. Resultant panel properties are calculated from the reaction force that acts on the fixed independent node of the zero-displacement MPC. The use of MPCs to distribute the forced displacement is a convenient way to represent a strengthened end of a sample and a rigid clamp, which would be used during standardized tensile testing or during rail shear tests. The displacements of the independent node of the MPC are either constrained entirely (in the case of a fixed side of the sample) or allowed to move only in the direction of forced displacement in the case of the edge subjected to forced displacement. The displacement constraint and forced displacement are distributed by the corresponding MPCs over the dependent nodes on the two edges of the mesh. This tensile and shear setup was validated using a monolithic composite plate of known properties, and the selected sample size ensures the edge effects are contained.

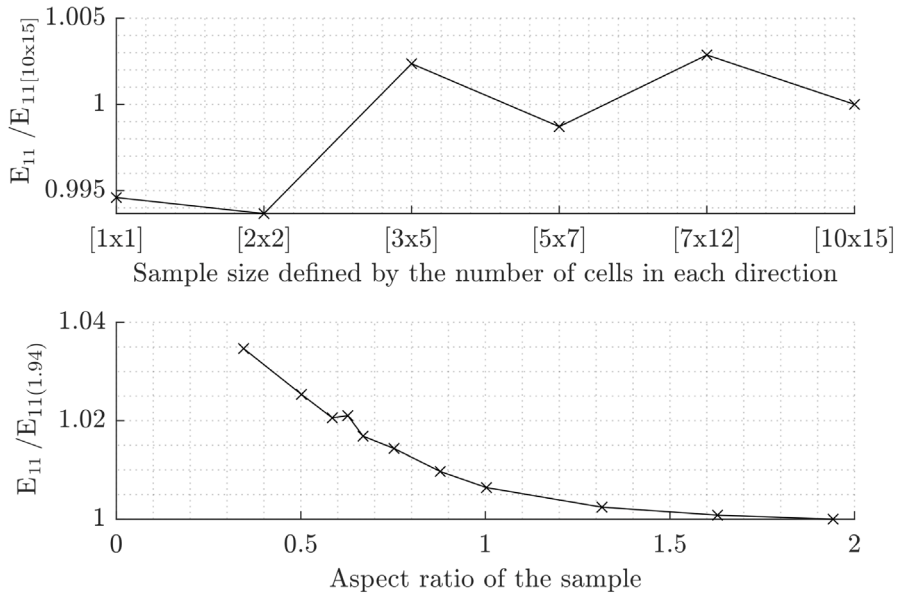

Fig. 4. Results of sample size sensitivity analysis. Values of Young's modulus in both graphs are normalized for clarity by dividing by the result of the largest sample. Number of cells are given in the direction of loading and perpendicular to it, respectively.

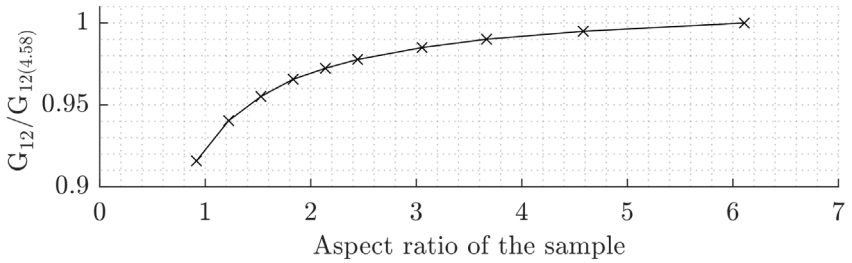

Fig. 5. Effect of sample aspect ratio on the resultant shear modulus. Shear modulus values are normalized by the result of the largest sample.

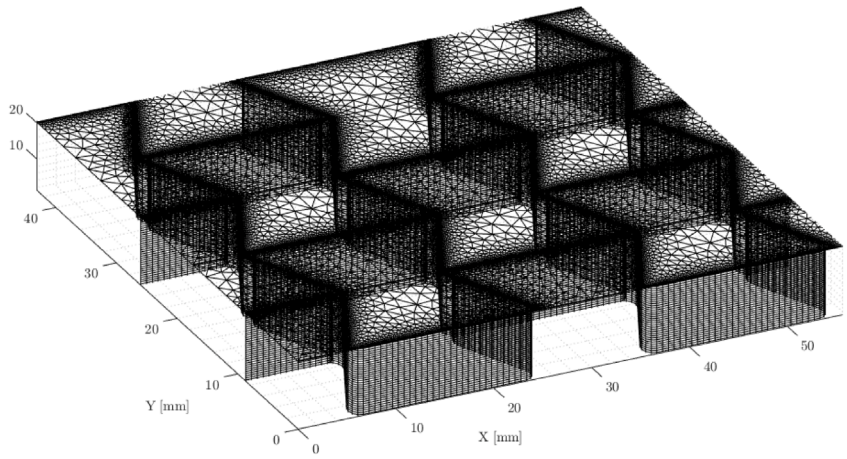

Fig. 6. The FE mesh of the sandwich panel. Lower skin is excluded to ensure the upper skin mesh is clearly visible.

3. Results and discussion

Results of the FE validation are presented using the difference between homogenized properties estimated using the proposed analytical approach and those obtained using the FE model of the same geometry. The first section demonstrates how the settings of the geometrical parameters of the core affect this difference and compares the effect with the findings of other authors. The second section describes the contribution of the core to the overall stiffness of the sandwich and shows its correlation with the difference between the two models, which allows us to draw general assumptions regarding the region of applicability of the proposed analytical approach. The scope of the article does not allow authors to present an individual evaluation of each parameter combination and each resulting property. Complete results for all the tested geometries, both Young's moduli, shear modulus, and both Poisson's ratios are available in an online repository [36].

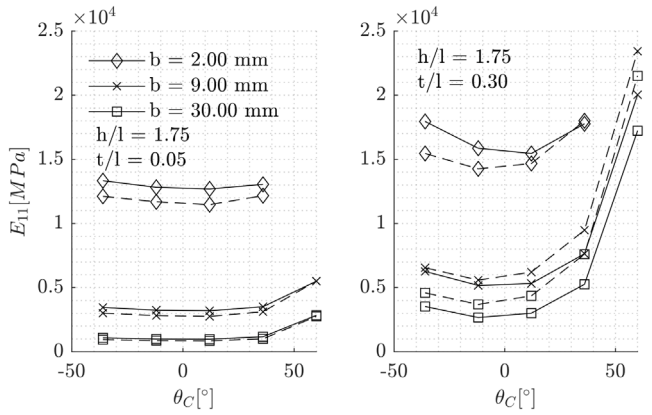

Fig. 7. Homogenized moduli E_{11} obtained using the two models for sample panels on a range of values of θ_C and b. The dashed line shows the analytical results, and the solid line shows the results of the FE analysis.

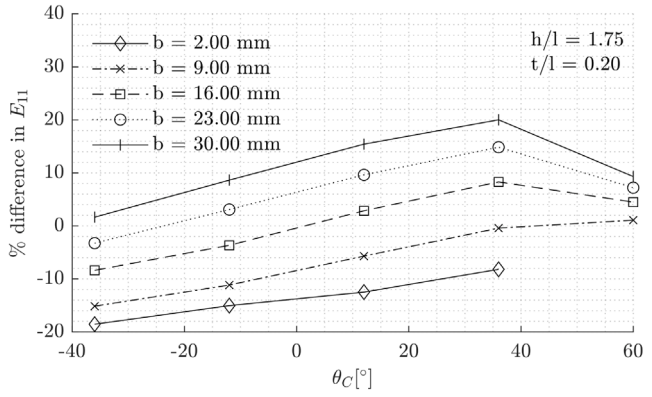

Fig. 8. Percentual difference between homogenized moduli E_{11} obtained using the two models for sample geometries with the t/l value closer to the center of the tested range.

3.1. Core thickness and cell angle

Plot in Fig. 7 shows the values of the homogenized modulus E_{11} obtained using the analytical model (dashed line) and FE model (solid line) for two combinations of t/l and h/l and a range of values of θ_C and b.

The left plot in Fig. 7 presents results for geometries with low cell wall thickness t/l and indicates the increase in the difference between the results of the two models corresponding to a decrease in core thickness b. This behavior can be explained by the concept of *core thickness effect* described by W. Becker [33] for regular honeycombs. Becker attributes an increase in the effective core stiffness of panels with a thinner core to the *coupling of the core displacements with those of the facesheets*.

This effect is omitted by the proposed beam-based analytical model, causing the analytical model to underestimate the E_{11} of panels with thinner cores. While this effect is evident on the panels with low relative wall thickness t/l, it becomes less significant on panels with thicker walls and higher cell angles θ_C, where the analytical model overestimates the E_{11} value (as shown in the right plot in Fig. 7). Closer to the middle of the tested range of the relative wall thickness, the percentual difference between the two models in Fig. 8 shows a transition between negative and positive difference and high dependency of the difference on both the cell angle θ_C and core thickness b.

Similar tendencies regarding the thickness effect can be seen in the results for the second Young's modulus E_{22} shown in Figs. 9 and 10. The difference between the models is higher than in the case of E_{11}, especially closer to the middle of the tested range of θ_C, where the highest difference reached 711%. In these cases, the honeycomb cell is close to a rectangular shape. The cell walls that are almost parallel to the loading direction are less prone to bending. Since the stretching of the wall does not become significant until $t/l = 1$ [25], the hinging of corner bends becomes the predominant mode of deformation. The used analytical model does not account for the corner hinging, which results in the large difference between the models.

The effect of hinging can be clearly seen in Fig. 11, which shows in-plane stress distribution on the two sides of a cell wall of the sample with the highest reached difference between models. Opposing orientation of the stresses shown by the markers and their comparable values signify that it is the stress associated with bending which drives the deformation. It should be also noted, that the second highly loaded area to the left of the marked one undergoes stress in the opposite direction than the marked one. This is caused by the combination of loading in the y direction and negative angle of cell θ_c.

Contrary to Becker's findings, shear modulus results (shown in Fig. 12) also follow the thickness effect in the same way as the samples with low wall thickness t/l in the case of E_{11}.

The same is true for Poisson's ratio results, but with differences between the models reaching extremely high values in cases with $\theta = -12°$ for ν_{12} and $\theta = 12°$ for ν_{21}, where the cells come close to a rectangular shape. Results for ν_{12} and ν_{21} can be found in [36].

3.2. Skin wall thickness

Figs. 13 and 14 show the effect of the change of relative cell wall thickness t/l and relative wall length (or cell elongation) h/l on the difference between models. Both E_{11} and E_{22}, as well as all the other tested properties show high dependency of the difference on the relative cell wall thickness t/l, which corresponds with results of Masters and Evans [25] and Balawi et al. [39], who suggested that the higher-density of honeycomb core drives the real properties of the core further from the simple 1D-beam-based predictions.

3.3. Contribution of the core to the overall stiffness

The majority of results show a high dependency of the difference between the two models on the stiffness of the core itself and its thickness — two parameters that can be tied together by using parameter α_N, representing the contribution of the core to the overall stiffness of the panel, defined as follows:

$$\alpha_{N1,2,3} = 1 - \frac{(E_{11SK}, E_{22SK}, G_{12SK})2t_c}{(E_{11N}, E_{22N}, G_{12N})(b + 2t_c)} \tag{19}$$

where $E_{11SK}, E_{22SK}, G_{12SK}$ are material properties of the skin, E_{11N}, E_{22N}, G_{12N} homogenized properties of the panel estimated using the FE model, and t_c is the skin thickness.

3.4. Selected samples

Crosses in Figs. 15, 16, and 17 mark the absolute difference between the results of the analytical model and FE results for all the tested sample panels. The horizontal axis of the figures represents the contribution of the core to the overall stiffness α_N. Larger symbols in the figures represent three selected samples that showed a high difference in one of the tested moduli. Geometrical parameters of these samples in Table 4 suggest that the core thickness b is the only common denominator between the three samples. Tracing each of the samples across Figs. 15, 16, and 17 shows that the differences obtained for one sample panel and different moduli vary greatly. This suggests that the difference observed across various moduli is influenced by different parameters, which makes it more difficult to estimate the limits of applicability of the proposed analytical approach.

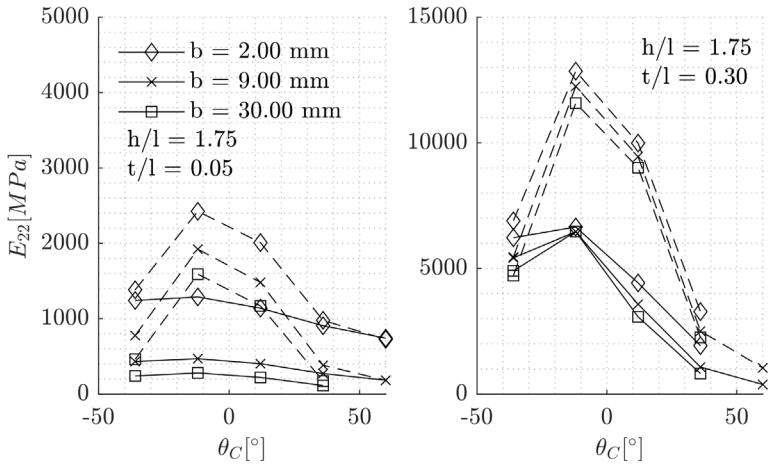

Fig. 9. Homogenized moduli E_{22} obtained using the two models for sample panels on a range of values of θ_C and b and two values of t/l. The dashed line shows the analytical results, and the solid line shows the results of the FE analysis.

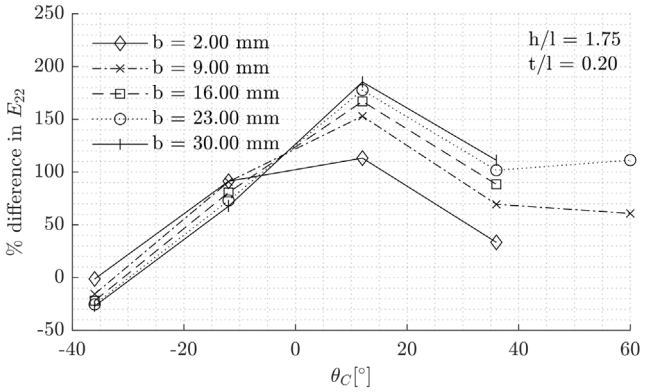

Fig. 10. Percentual difference between homogenized moduli E_{22} obtained using the two models for sample geometries with the t/l value closer to the center of the tested range.

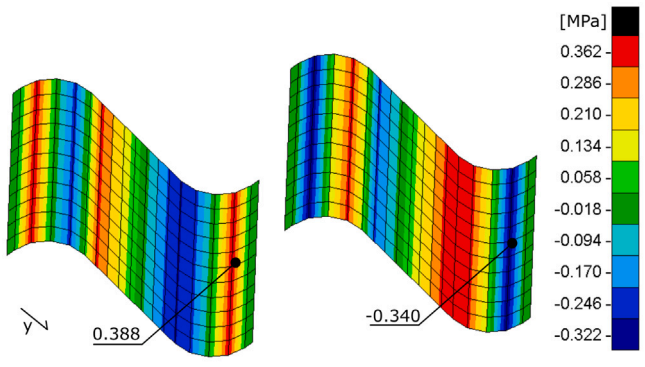

Fig. 11. In-plane stress on the two sides of the cell wall of sample #143 during estimation of E_{22} by loading the sample in the Y direction.

Table 4
Selected samples.

Sample	Symbol	h/l	t/l	b	θ_C
#25	●	3	0.1	30	−60
#143	■	0.5	0.05	30	−12
#233	♦	0.5	0.3	30	12

3.5. Omitting the core stiffness

Use of the core thickness b as a sole optimization parameter of the core and subsequent omission of the core in-plane stiffness in the analytical representation of the sandwich is one of the most common simplifications in aerospace applications. This simplification approaches the core as a middle layer that increases the effective thickness of the panel (increasing its bending stiffness), but does not contribute to the in-plane stiffness of the panel (rendering the effective in-plane stiffness of the panel equal to the stiffness of the faces). Dots in the Figs. 15, 16, and 17 show the absolute difference between the results of this core-omitting approach and the results of FE analysis for each of the tested sample panels.

The results of E_{11} and G_{12} show a slight advantage of the proposed analytical model, with only a few cases with differences higher than the core-omission results. Results of E_{22} show significantly lower precision of the proposed analytical model and although for more than half of the sample panels the use of analytical model results in a better match with the FEA results, some of the remaining cases show multiple times higher differences making it possible to argue that the omission of the core can in this case lead to both more precise and more predictable results.

3.6. Analytically predicted contribution of the core

Trends described in the previous sections suggest a general tendency of the difference between models to increase with an increase in the homogenized stiffness of the core and also with the ratio with which the core contributes to the overall stiffness of the sandwich. The contribution of the core to the sandwich stiffness can be predicted using the proposed analytical approach, and relating the difference between the results of the two models to the prediction enables us to roughly estimate the difference without relying on the FE results. Considering the FE model results closely match the properties of a real panel, the predicted contribution of the core allows us to estimate how closely the proposed analytical approach represents the properties of a real panel.

Using the homogenized properties of the sandwich panel E_{11A}, E_{22A}, G_{12A}, and the homogenized properties of the core E_{11C}, E_{22C}, G_{12C}, estimated by the analytical model, the core contribution can be predicted as:

$$\alpha_{A1,2,3} = \frac{(E_{11C}, E_{22C}, G_{12C})b}{(E_{11A}, E_{22A}, G_{12A})(b + 2t_c)} \tag{20}$$

This allows plotting the dependency of the difference between models on the predicted contribution of the core as shown in Figs. 18, 19, and 20.

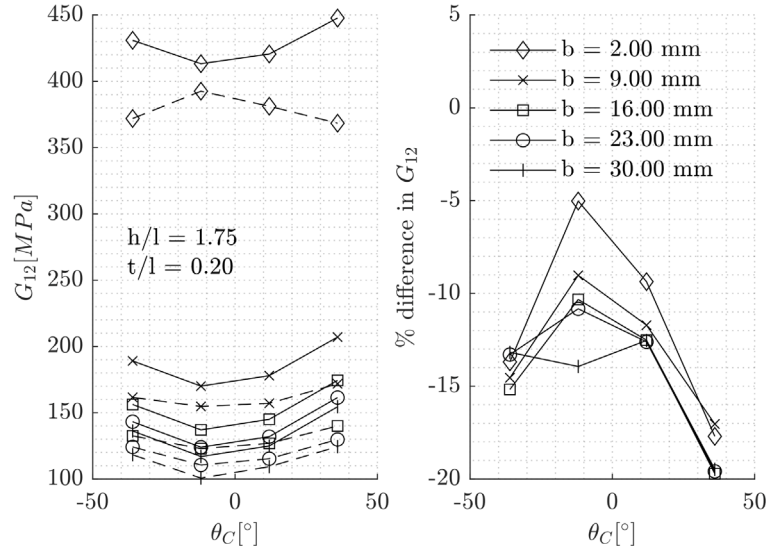

Fig. 12. Difference between homogenized shear moduli G_{12} obtained using the two models for sample panels with one combination of t/l and h/l. The dashed line in the left figure shows the analytical results, and the solid line shows the results of the FE analysis.

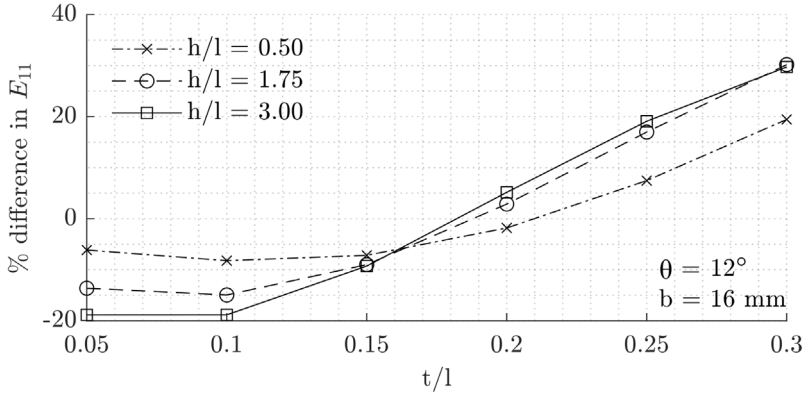

Fig. 13. Difference between homogenized moduli E_{11} obtained using the two models for sample panels with one combination of θ_C and b and different values of t/l and h/l.

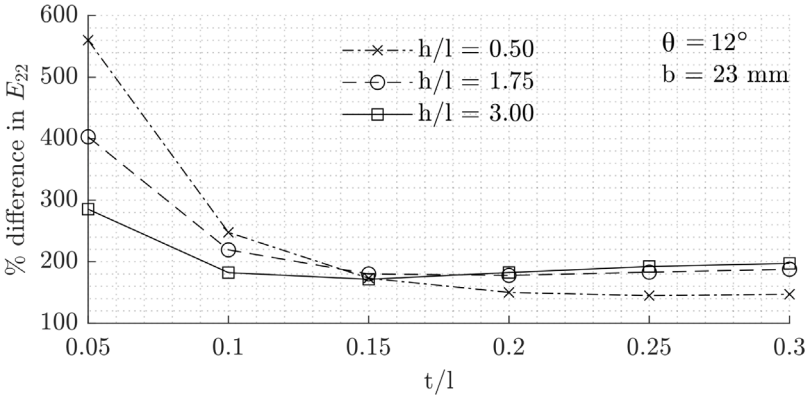

Fig. 14. Difference between homogenized moduli E_{22} obtained using the two models for sample panels with one combination of θ_C and b and different values of t/l and h/l.

E_{11} prediction in Fig. 18 does not rise above 23% difference up to $\alpha_{A1} = 0.51$, creating a region with reasonable precision of the analytical model. In case of E_{22}, this region is almost nonexistent with the difference reaching above 30% at $\alpha_{A2} = 0.12$, and although the model still reaches a lower difference from FE results than omitting the core E_{22} altogether, benefits of its use are arguable. A similar conclusion can be said about the precision of G_{12} prediction in Fig. 20, which reaches 20% difference at $\alpha_{A3} = 0.04$ and follows with a long flat region with almost constant precision across the whole tested spectrum of α_{A3}. Overlying box plots in the figures provide better insight into the

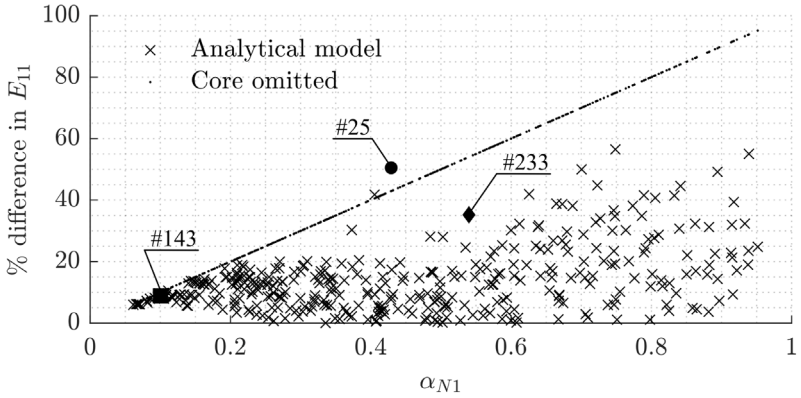

Fig. 15. Comparison of analytical model and core-omitting approach for E_{11}.

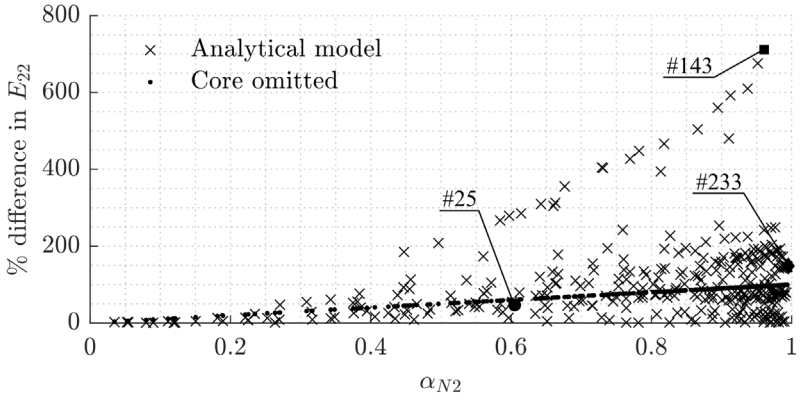

Fig. 16. Comparison of analytical model and core-omitting approach for E_{22}.

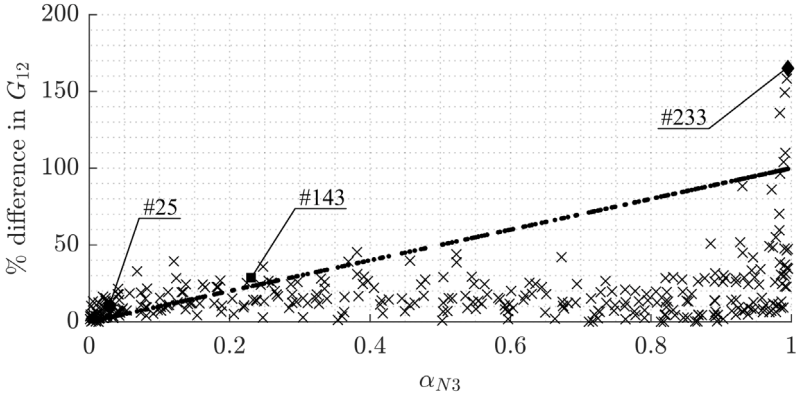

Fig. 17. Comparison of analytical model and core-omitting approach for G_{12}.

distribution of the results. Boxes represent the values of the 25th and 75th percentiles, and whiskers show an interval of $\pm 2\sigma$. This interval in Figs. 19 and 20 shows that although in the extremes the difference between models can reach over 700%, for most cases it does not reach over half of these extreme values.

3.7. Impact of the analytical model precision on the optimization results

General impact of the analytical model precision on results of an optimization of a complex structure is difficult to assess due to high computational efforts involved in detailed numerical modeling of the sandwich panel structures. Nevertheless, since the main motivation for implementing sandwich panels into optimization is to avoid weight penalties associated with buckling, some conclusions can be drawn from estimating the impact on the critical buckling load N_0 of a typical skin panel of an aircraft wing.

The critical loads, parallel to the longer edge of the panel, are estimated as described by Kassapoglou et al. in [12] for buckling of a rectangular composite plate under uniaxial compression load. An example panel was chosen from a midspan of the NASA Common Research Model wing [40], which is often used as a benchmark optimization case study [16,28]. The dimensions of this rectangular buckling panel are defined by the distance between the ribs and the pitch of the stringers as 550 and 144 mm, respectively. This panel is assigned with the homogenized stiffness properties estimated by the two models for panel samples #143 and #27, samples which showed the largest positive and

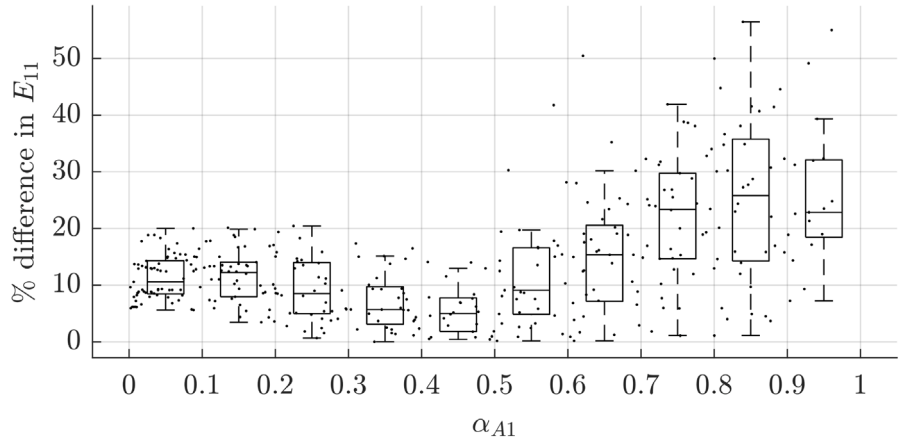

Fig. 18. Dependency of the precision of analytical estimation of E_{11} on the predicted contribution of the core. Boxes represent the values of 25th and 75th percentiles, and whiskers show an interval of $\pm 2\sigma$.

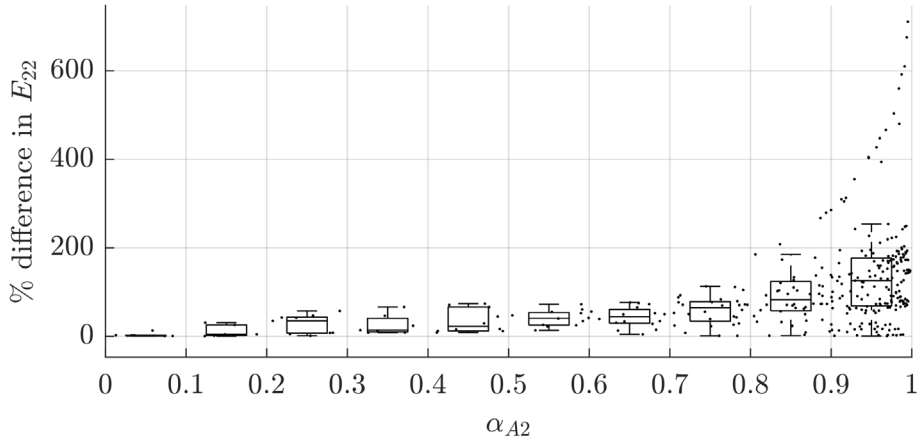

Fig. 19. Dependency of the precision of analytical estimation of E_{22} on the predicted contribution of the core. Boxes represent the values of 25th and 75th percentiles, and whiskers show an interval of $\pm 2\sigma$.

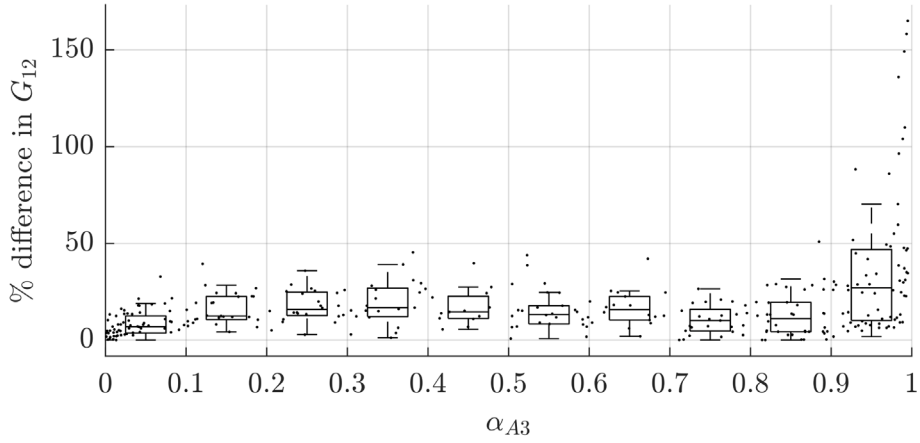

Fig. 20. Dependency of the precision of analytical estimation of G_{12} on the predicted contribution of the core. Boxes represent the values of 25th and 75th percentiles, and whiskers show an interval of $\pm 2\sigma$.

negative differences. The largest difference between the results of both models (In Table 5) occurred in the 2nd material direction. To access the least favorable option, this direction was aligned with the loading direction.

Results in Table 5 show that although the difference in the critical buckling load N_0 is less than the difference between the E_{22}, the value is still significant. Considering the analytical model is used as a part of the optimization process, the 64.7% difference in the prediction of buckling load in sample #143 would lead to an unrealistically optimistic design with a significantly decreased reserve factor, while the negative difference of 42.5% in the second case causes an overly conservative result and unnecessary increase in weight.

Table 5
Critical buckling loads of the CRM panel.

Sample	E_{22} diff.	N_0 diff.
#143	+711%	+64.7%
#27	−73%	−42.5%

4. Conclusions

This study presented an analytical approach that uses a combination of CLT and a beam-based model to predict the homogenized mechanical properties of sandwich panels with honeycomb core. A novel approach to model validation based on script-generated FE models was used to determine homogenized properties of 425 panels with different core geometries and compare them with the results of the analytical model.

Results helped to identify the influence of different core parameters on the difference between the analytical and numerical results. Some of these influences (such as the core thickness effect) were already observed by other authors. Nevertheless, some of the previous observations were based on a narrow spectrum of samples, and the presented results of the validation put them into a broader context.

Although the proposed analytical model is capable of estimating the desired properties across the whole tested range of parameters, the difference between analytical and numerical results varies greatly — from a difference of a few percent to more than 700%.

Results also showed that the difference could not be directly correlated with either of the tested geometrical parameters of the core, but rather resulted from their varying combinations. Nevertheless, the difference showed a high dependency on the contribution of the core to the overall stiffness of the sandwich, and this dependency can be used to roughly estimate the expected precision for different samples and determine the general limits of applicability of the model.

The mean values of the absolute difference between the models across the whole tested spectrum were 13.9%, 107.2%, and 18.6% for E_{11}, E_{22}, and G_{12}, respectively. To put these values into perspective, the analytical results were compared with the results of a different analytical approach that omits the in-plane stiffness of the core altogether — a simplification commonly employed in preliminary design applications in the aerospace field. The proposed analytical approach delivered better results for most of the samples.

In the context of sandwich optimization, both E_{11} and G_{12} show a precision sufficient for analysis or optimization of a preliminary design on a relatively broad region of applicability, which can be defined using the analytical prediction of the core contribution to overall stiffness of the sandwich. The results for modulus E_{22} and their impact on critical buckling load prediction make the practicality of use of the analytical model for E_{22} prediction debatable.

A significant broadening of the design space available to the optimizer and a more reasonable prediction of E_{22} could be achieved by a detailed study of the mentioned effects and creating a more comprehensive model of the behavior of the honeycomb core. Here, the proposed FE validation approach could serve as a useful tool.

The performed validation was conducted using an aluminium core and unidirectional CFRP skins. Nevertheless the same analytical modeling approach can be applied for the prediction of homogenized properties of sandwich panels with honeycomb cores made of other materials, such as aramid-based composites, and different skin layouts and materials, including non-symmetric and unbalanced laminates. However, it should be noted that the validation was conducted using unidirectional single-ply skins with constant layout and thickness. Although the use of the normalized core contribution parameter allows for generalizing the findings to quasi-isotropic and orthotropic skins of varying thicknesses, generalization of the findings to more complex non-symmetric and unbalanced laminate skins should be done with caution.

More concise results of mechanical property prediction could also be achieved by using a core material that is less susceptible to changes in modes of deformation with a change of cell geometry. Since most of the effects noted in the study can be associated with any 2-D lattice structure used as a sandwich core, the optimization could potentially benefit from the use of 3D mechanical metamaterials, whose properties are based on 3-dimensional cells, rather than a 2D lattice.

CRediT authorship contribution statement

Vladimír Hostinský: Writing – original draft, Validation, Software, Conceptualization. **Jurij Sodja:** Writing – review & editing, Supervision, Resources, Methodology, Funding acquisition. **Ivo Jebáček:** Writing – review & editing, Supervision, Resources, Project administration. **Jan Navrátil:** Writing – review & editing, Supervision, Funding acquisition, Conceptualization.

Declaration of competing interest

The authors declare that they have no known competing financial interests or personal relationships that could have appeared to influence the work reported in this paper.

Acknowledgments

This research was funded by the European Union under Horizon Europe Grant Agreement number 101079091 – BAANG and the project No. FSI-S-23-8163 funded by The Ministry of Education, Youth and Sport (MEYS, MŠMT in Czech) institutional support.

Data availability

Data repository containing the dataset supporting the study can be found under DOI:10.5281/zenodo.14229746 and the software, which was created for the model validation is available under DOI:10.5281/zenodo.18377054.

References

[1] Mcdonald RA, German BJ, Takahashi T, Bil C, Anemaat W, Chaput A, Vos R, Harrison N. Future aircraft concepts and design methods. Aeronaut J 2022;126(1295):92–124. http://dx.doi.org/10.1017/aer.2021.110.

[2] Bravo-Mosquera PD, Catalano FM, Zingg DW. Unconventional aircraft for civil aviation: A review of concepts and design methodologies. 2022, http://dx.doi.org/10.1016/j.paerosci.2022.100813.

[3] Bradley MK, Droney CK. Subsonic ultra green aircraft research: Phase II-volume II-hybrid electric design exploration. Tech. rep., NASA; 2015.

[4] Towards a Sustainable Air Transportation System. In: Whitepaper. Tech. rep., TU Delft, NLR; 2021.

[5] Chakraborty I, Nam T, Gross JR, Mavris DN, Schetz JA, Kapania RK. Comparative assessment of strut-braced and truss-braced wing configurations using multidisciplinary design optimization. J Aircr 2015;52(6):2009–20. http://dx.doi.org/10.2514/1.C033120, URL https://arc.aiaa.org/doi/10.2514/1.C033120.

[6] Ma Y, Abouhamzeh M, Elham A. Geometrically nonlinear coupled adjoint aerostructural optimization of natural-laminar-flow strut-braced wing. J Aircr 2023;60(3):935–54. http://dx.doi.org/10.2514/1.C036988.

[7] Sohst M, Lobo do Vale J, Afonso F, Suleman A. Optimization and comparison of strut-braced and high aspect ratio wing aircraft configurations including flutter analysis with geometric non-linearities. Aerosp Sci Technol 2022;124. http://dx.doi.org/10.1016/j.ast.2022.107531.

[8] Weishaar T. Aeroelastic tailoring - Creative uses of unusual materials. In: 28th structures, structural dynamics and materials conference. Reston, Virigina: American Institute of Aeronautics and Astronautics; 1987, http://dx.doi.org/10.2514/6.1987-976.

[9] Brooks TR, Martins JR, Kennedy GJ. High-fidelity aerostructural optimization of tow-steered composite wings. J Fluids Struct 2019;88:122–47. http://dx.doi.org/10.1016/J.JFLUIDSTRUCTS.2019.04.005.

[10] Wang Z, Wan Z, Groh RM, Wang X. Aeroelastic and local buckling optimisation of a variable-angle-tow composite wing-box structure. Compos Struct 2021;258. http://dx.doi.org/10.1016/j.compstruct.2020.113201.

[11] Sodja J, Werter NPM, De Breuker R. Aeroelastic demonstrator wing design for maneuver load alleviation under cruise shape constraint. J Aircr 2021;58(3):448–66. http://dx.doi.org/10.2514/1.c035955.
[12] Kassapoglou C, Belobaba P, Cooper J, Langton R, Seabridge A. Design and analysis of composite structures. 2nd ed.. Wiley; 2013.
[13] Ashby M, Bréchet Y. Designing hybrid materials. Acta Mater 2003;51(19):5801–21. http://dx.doi.org/10.1016/S1359-6454(03)00441-5.
[14] Jin P, Song B, Zhong X, Yu T, Xu F. Aeroelastic tailoring of composite sandwich panel with lamination parameters. Proc Inst Mech Eng G 2016;230(1):105–17. http://dx.doi.org/10.1177/0954410015587724.
[15] Hegberg T. Fast aeroelastic analysis and optimisation of large mixed materials wind turbine blades (Ph.D. thesis), TU Delft; 2019, http://dx.doi.org/10.4233/uuid:643ddf12-97d3-48a1-9742-b4dd22f16164.
[16] Meddaikar YM, Dillinger JK, Silva GH, De Breuker R. Skin panel optimization of the common research model wing using sandwich composites. J Aircr 2022;59(2):386–99. http://dx.doi.org/10.2514/1.C036551.
[17] Jin P, Zhong X. Flutter characteristic study of composite sandwich panel with functionally graded foam core. Int J Aerosp Eng 2016;2016. http://dx.doi.org/10.1155/2016/7971435.
[18] Zadpoor AA. Mechanical meta-materials. Mater Horizons 2016;3(5):371–81. http://dx.doi.org/10.1039/C6MH00065G.
[19] Schaedler TA, Carter WB. Architected cellular materials. 2016, http://dx.doi.org/10.1146/annurev-matsci-070115-031624.
[20] Krushynska AO, Torrent D, Aragón AM, Ardito R, Bilal OR, Bonello B, Bosia F, Chen Y, Christensen J, Colombi A, Cummer SA, Djafari-Rouhani B, Fraternali F, Galich PI, Garcia PD, Groby JP, Guenneau S, Haberman MR, Hussein MI, Janbaz S, Jiménez N, Khelif A, Laude V, Mirzaali MJ, Packo P, Palermo A, Pennec Y, Picó R, López MR, Rudykh S, Serra-Garcia M, Sotomayor Torres CM, Starkey TA, Tournat V, Wright OB. Emerging topics in nanophononics and elastic, acoustic, and mechanical metamaterials: An overview. 2023, http://dx.doi.org/10.1515/nanoph-2022-0671.
[21] Surjadi JU, Gao L, Du H, Li X, Xiong X, Fang NX, Lu Y. Mechanical metamaterials and their engineering applications. Adv Eng Mater 2019;21(3). http://dx.doi.org/10.1002/ADEM.201800864.
[22] Gibson LJ, Ashby MF, Schajer GS, Robertson CI. The mechanics of two-dimensional cellular materials. Proc R Soc A 1982;382(1782):25–42. http://dx.doi.org/10.1098/rspa.1982.0087.
[23] Froud GR. Your sandwich order, Sir? Composites 1980;11(3):133–8.
[24] Malek S, Gibson L. Effective elastic properties of periodic hexagonal honeycombs. Mech Mater 2015;91(P1):226–40. http://dx.doi.org/10.1016/j.mechmat.2015.07.008.
[25] Masters IG, Evans KE. Models for the elastic deformation of honeycombs. Compos Struct 1996;35:403–22.
[26] Balawi S, Abot JL. A refined model for the effective in-plane elastic moduli of hexagonal honeycombs. Compos Struct 2008;84(2):147–58. http://dx.doi.org/10.1016/j.compstruct.2007.07.009.
[27] Silva GH, Meddaikar Y. Lamination parameters for sandwich and hybrid material composites. AIAA J 2020;58(10):4604–11. http://dx.doi.org/10.2514/1.J059093.
[28] Werter NP, De Breuker R. A novel dynamic aeroelastic framework for aeroelastic tailoring and structural optimisation. Compos Struct 2016;158:369–86. http://dx.doi.org/10.1016/J.COMPSTRUCT.2016.09.044.
[29] Brooks TR, Kennedy G, Martins JRRA. High-fidelity aerostructural optimization of a high aspect ratio tow-steered wing. In: 57th AIAA/ASCE/AHS/ASC structures, structural dynamics, and materials conference. Reston, Virginia: American Institute of Aeronautics and Astronautics; 2016, http://dx.doi.org/10.2514/6.2016-1179.
[30] Macquart T, Werter N, De Breuker R. Aeroelastic design of blended composite structures using lamination parameters. J Aircr 2017;54(2):561–71. http://dx.doi.org/10.2514/1.C033859.
[31] Tsai SW, Pagano NJ. Invariant properties of composite materials. Tech. rep., Air Force Materials Laboratory; 1968, URL https://apps.dtic.mil/sti/pdfs/AD0668761.pdf.
[32] Barbero EJ. Introduction to second edition. Tech. rep..
[33] Becker W. Closed-form analysis of the thickness effect of regular honeycomb core material. Compos Struct 2000;48(1–3):67–70. http://dx.doi.org/10.1016/S0263-8223(99)00074-4.
[34] Gibson LJ, Ashby MF. Cellular solids. In: Cellular solids: structure and properties, second edition. Cambridge University Press; 1997, p. 1–510. http://dx.doi.org/10.1017/CBO9781139878326.
[35] Box GeorgeEP. Statistics for experimenters. Wiley-Interscience; 1978.
[36] Hostinský V. Validation of an analytical model of a sandwich panel. 2025.
[37] Persson P-O, Strang G. A simple mesh generator in MATLAB. Tech. rep., MIT; 2004, URL [https://persson.berkeley.edu/pub/persson04mesh_col.pdf].
[38] Field DA. Qualitative measures for initial meshes. Internat J Numer Methods Engrg 2000;47(4):887–906. http://dx.doi.org/10.1002/(SICI)1097-0207(20000210)47:4<887::AID-NME804>3.0.CO;2-H.
[39] Balawi S, Abot JL. The effect of honeycomb relative density on its effective in-plane elastic moduli: An experimental study. Compos Struct 2008;84(4):293–9. http://dx.doi.org/10.1016/j.compstruct.2007.08.009.
[40] Vassberg JC, DeHaan MA, Rivers MS, Wahls RA. Retrospective on the common research model for computational fluid dynamics validation studies. J Aircr 2018;55(4):1325–37. http://dx.doi.org/10.2514/1.C034906, American Institute of Aeronautics and Astronautics Inc..